Organic Electronics 13 (2012) 1916–1924

Contents lists available at SciVerse ScienceDirect

Organic Electronics

journal homepage: www.elsevier.com/locate/orgel

# Low frequency dielectric loss of metal/insulator/organic semiconductor junctions in ambient conditions

R. Ledru [a], S. Pleutin [a,b,*], B. Grouiez [a], D. Zander [a], H. Bejbouji [a,b], K. Lmimouni [b], D. Vuillaume [b]

[a] CReSTIC, University of Reims, Moulin de la Housse, F-51687 Reims Cedex 2, France
[b] Institute for Electronics, Microelectronics and Nanotechnology (IEMN), CNRS, University of Lille, BP 60069, Avenue Poincaré, Villeneuve d'Ascq, F-59652 Cedex, France

ARTICLE INFO

*Article history:*
Received 21 December 2011
Received in revised form 25 March 2012
Accepted 8 April 2012
Available online 20 June 2012

*Keywords:*
Metal–oxide–organic semiconductor junctions
Dielectric relaxation
Anomalous diffusion
Admittance spectroscopy

ABSTRACT

The complex admittance of metal/oxide/pentacene thin film junctions is investigated under ambient conditions. At low frequencies, a contribution attributed to proton diffusion through the oxide is seen. This diffusion is shown to be anomalous and is believed to be also at the origin of the bias stress effect observed in organic field effect transistors. At higher frequencies, two dipolar contributions are evidenced, attributed to defects located one at the organic/oxide interface or within the organic, and the other in the bulk of the oxide. These two dipolar responses show different dynamic properties that manifest themselves in the admittance in the form of a Debye contribution for the defects located in the oxide, and of a Cole–Cole contribution for the defects related to the organic.



## 1. Introduction

As Organic Field-Effect Transistors (OFET) are now close to applications, questions about their reliability under realistic atmospheric conditions become more and more important [1]. Electrical instabilities are evidenced, for instance, in the bias stress effect where under a prolonged application of a gate potential the device characteristics, such as the threshold voltage, evolve with time [1,2]. Several mechanisms were proposed to understand these degradations of the device properties. Some are intrinsic mechanisms such as trapping of charges, in the organic film [3–5] or at the organic/oxide interface [6], or pairing of mobile charges to heavier bipolarons [7]. Some others are extrinsic mechanisms needed especially when the measurements are done in the air since humidity was shown to amplify these instabilities [8]. An example of such mechanism was proposed recently based on proton production by electrochemical reactions involving water molecules adsorbed at the organic/oxide interface, followed by proton diffusion through the oxide [9,10].

We have considered $Si^{+}/SiO_2$/pentacene/Au junctions that are the two terminal pendants of thin film transistors with the same layer structure. We study the dynamic electrical response of these junctions under ambient conditions over a large frequency window as function of a superimposed dc voltage ($V_{dc}$). This technique has proven in the past to be powerful because of its sensitivity and its ability to separate the different process involved [11,12]. It was already applied to several organic based junctions [13,14] but the results were interpreted based on models relying on the Shokley–Read–Hall statistics not appropriated to organic materials [11,12]. Compared to these previous works [13,14] our frequency range is more extended, going down to $10^{-1}$ Hz, and the analysis of our data insist on the crucial role played by the interactions of the defects with their surroundings which determine the shape of the measured response functions [15–18]. We have identified two types of defects

* Corresponding author at: Institute for Electronics, Microelectronics and Nanotechnology (IEMN), CNRS, University of Lille, BP 60069, Avenue Poincaré, Villeneuve d'Ascq, F-59652 Cedex, France.
*E-mail address:* stephane.pleutin@isen.iemn.univ-lille1.fr (S. Pleutin).

1566-1199/$ - see front matter © 2012 Elsevier B.V. All rights reserved.
http://dx.doi.org/10.1016/j.orgel.2012.04.035

with different dynamic properties: one located inside the oxide shows a Debye type of response, the other located at the oxide/organic interface, or in the bulk of the organic, shows a Cole–Cole type of response [17,19,20]. At lower frequencies (<100 Hz) we observe anomalous Low Frequency Dispersion (LFD) [21] that is consistent with the ionic diffusion current proposed in Refs. [9,10] but instead of normal diffusion considered in these works, our results evidence fractional diffusion to occur [22,23].

## 2. Materials and methods

### 2.1. Device preparation

The samples are fabricated using 70 (±7) nm thick $SiO_2$ layer which was thermally grown on a heavy phosphorus doped n-typed silicon (100) (0.001–0.003 Ω cm). Prior to the pentacene deposition, the substrate was cleaned in an ultrasonic bath with acetone and isopropanol, and then blown with dry nitrogen. Subsequently, it was exposed to UV-ozone for 20 min. Then the thermal evaporation of the 40 nm thick pentacene organic active layer was done under the base pressure of $2.8–3 \times 10^{-6}$ mbar. The deposition rate of pentacene was maintained at 0.1 Å/s on the substrate kept at room temperature. After the deposition of the pentacene, the sample was transferred to the metallization chamber in order to deposit 120 nm of gold electrodes.

### 2.2. Admittance measurements

We have considered about 20 devices in ambient conditions showing all the same qualitative features. We present below results mostly for one of then that is very representative. For each sample, a small part of the surface is left free of pentacene. This allows us to access on the $Si^+/SiO_2$/Au junctions that constitute the "reference" measurements which can be compared with the organic based systems. We have measured the admittance in the frequency range $10^{-1}$–$10^5$ Hz as function of a static potential ($V_{dc}$) varying between −20 and +20 V. The $V_{dc}$ bias and the small superimposed $V_{ac}$ signal (100 mV) was applied to the gold electrode. Three different sizes of $9 \times 10^{-4}$, $3.6 \times 10^{-3}$ and $10^{-2}$ cm$^2$ of contact electrode were accessible on our devices but no size effects were noticed. The complex admittance, $Y(\omega)$, was measured using a frequency response analyzer (Solartron 1260) coupled with an interface dielectric (Solartron 1296) that provides directly the parallel conductance and capacitance. We write the response as [16]:

$$\frac{Y(\omega)}{\omega} = j(C'(\omega) - j(C''(\omega)) = j(\chi'(\omega) + C_\infty) + \chi''(\omega), \qquad (1)$$

where all the terms are supposed to be normalized by the contact surface area. As usual, we define $\omega = 2\pi f$, $f$ the signal frequency. $C'$ contains information about the polarization properties, $C''$ about the energy dissipated by the system during the polarization process. $C_\infty$ is the part of the capacitance that includes the response of the "fast" species (electrons, polarons, phonons, etc.) able to follow instantaneously the electric field (considering our frequencies range). In other words, it is the capacitance of an ideal junction (junction without defects) for which the amplitude is fixed, as in standard metal/oxide/semiconductor junctions, by the density profile of the free carriers present in the semiconductor. At the frequencies considered in this work, the electric energy is transferred without any loss to the free carriers and therefore $C_\infty$ is a real quantity. $\chi$ is the part of the dielectric susceptibility that includes the response of the "slow" species present in the junctions. They could be slow ions, defects able to trap free carriers or impurities carrying permanent dipoles, for instance. In other words, $\chi$ includes the response of various defects that contribute to increase the ideal capacitance, $C_\infty$, by adding new mechanisms of polarization but which dissipate part of the electric energy in the surrounding. $\chi$ is therefore a complex quantity: the real part describes the polarization processes of the defects, the imaginary part the way part of the electric energy is lost.

## 3. Results and discussion

Typical results are shown in Fig. 1a and b giving $C'$ and $C''$, respectively, for different dc voltages ($V_{dc}$). The results for a corresponding reference junction are also shown on the same graphs. These results show a loss part (Fig. 1b) structured and weakly frequency dependent with a minimum loss $\sim 10^{-10}$ S s cm$^{-2}$ ($\tan\delta$ about $10^{-3}$) [20]. As for all the junctions that we have investigated, our data clearly show that the admittance is decomposed in two qualitatively different types of independent contributions (see Fig. 1). The first type of contributions $\chi_{Ion}$ observed at low frequencies (<100 Hz) for all of our devices shows a decrease both in the real and the imaginary part of $Y(\omega)/\omega$ following a fractional power law. We identify this contribution with a LFD observed in systems where the polarization is controlled by currents of slow charges [21]. The second type of contribution ($10^2$–$10^5$ Hz) is dipolar type that manifests itself as a peak in the loss part of the admittance [16,17,20]. Our data are very well reproduced if we consider only two different dipolar contributions $\chi_{Organic}, \chi_{SiO_2}$. Because they are visible for different range of $V_{dc}$ they can be attributed to defects located one in the bulk of the $SiO_2$ and the other on the organic/oxide interface or within the organic film. The dielectric susceptibility of Eq. (1) is then written as a sum of three components

$$\chi(\omega) = \chi_{SiO_2}(\omega) + \chi_{Organic}(\omega) + \chi_{Ion}(\omega). \qquad (2)$$

The relative amplitude of each of these components fluctuates from device to device and varies with $V_{dc}$. We do the same analysis for the "reference" junctions for which no contribution of the pentacene appears. In the example of Fig. 1, the reference junction shows clearly an ionic but no sizable dipolar contribution. Indeed, for frequencies above 10 Hz the imaginary part of the dielectric susceptibility becomes so weak to reach the sensitivity limitation of our experiment resulting in the wide fluctuations shown in Fig. 1b. For frequencies above 10 Hz, the capacitance of this reference junction is then close to the

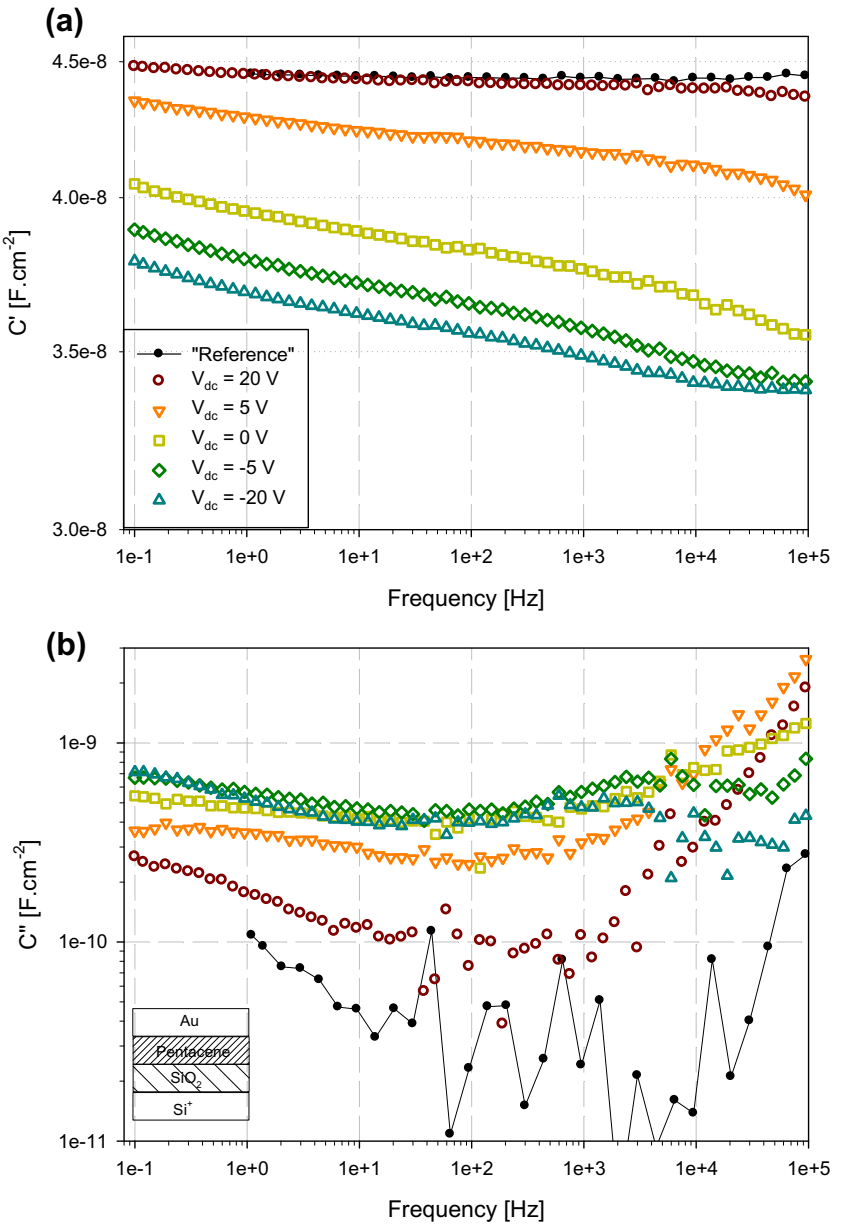


**Fig. 1.** Typical capacitance, (a) real part, $C$, and (b) imaginary part, $C$, for $V_{dc}$ = 20 V to −20 V. Results for the reference junction at $V_{dc}$ = 0 V are also shown (dots). Insert of (b): schematic of the layer structure of the junctions.

geometric capacitance. Another example of reference junction, with more pronounced dipolar contribution, will be shown later.

The three contributions of Eq. (2) are detailed farther. In particular, simple analytic expressions for each of these three contributions are given Eqs. (3), (4), and (7). With the Eqs. (1) and (2), together with these analytic expressions, we accurately fit the complex admittance at every $V_{dc}$ as will be seen below (examples are shown in Figs. 3 and 4, for specific values of $V_{dc}$). In particular, the fitting procedure gives us the $C_\infty - V_{dc}$ curves that we first comment before presenting the different contributions of Eq. (2).

### 3.1. $C_\infty - V_{dc}$ characteristics

An example of $C_\infty - V_{dc}$ curves that corresponds to the measurements of Fig. 1 is shown in Fig. 2. This quantity contains only the contributions of the fast degrees of freedom (hole, polarons, etc.) to the polarization and gives information about the electrostatic properties of a pure junction where all the slow contributions contained in $\chi$ have been removed.

The infinite frequency capacitance of the "reference" junctions has been shown to be bias independent, as it should be, and shows good agreements with the theoretical expectations: the case of Fig. 1a, for instance, corresponds

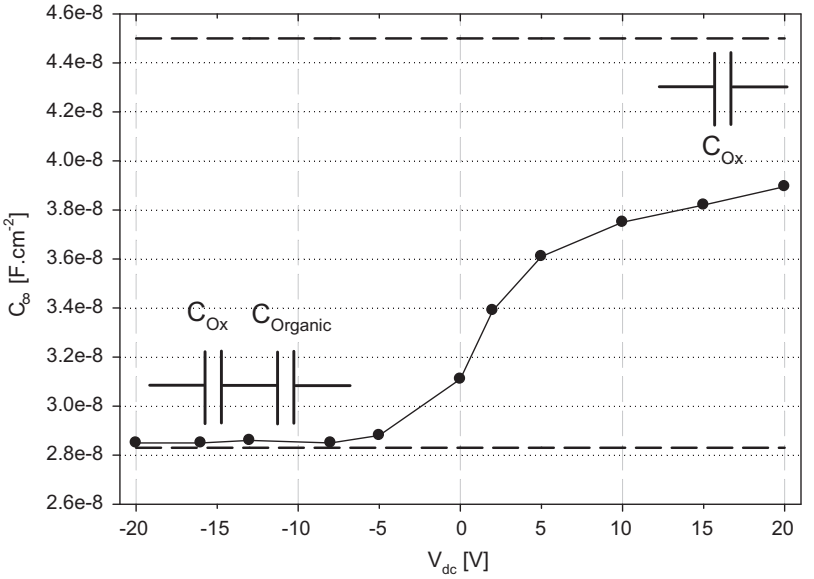


**Fig. 2.** Infinite frequency capacitance, $C_\infty$, extracted from the results shown in Fig. 1 following the fitting procedure described in the text, as function of $V_{dc}$. The two limiting values are also shown. The upper limit is the capacitance in the full accumulation regime that corresponds to the infinite capacitance of the corresponding reference junction, $C_{Ox}$. The lower limit is the capacitance in the full depletion regime given by the capacitance of a 40 nm layer of pentacene (with $\varepsilon = 3.5$), $C_{Organic}$, and $C_{Ox}$ in series.

to an oxide of 77 nm width once the frequency dependant part of the admittance has been subtracted (see Fig. 2). The $C_\infty - V_{dc}$ curves of the pentacene based junctions (an example is shown in Fig. 2) appear to be similar to the ones of classical metal/oxide/semiconductor junctions but we have to keep in mind that the organic semiconductors differ noticeably from their inorganic counter part [24,25]. First, the organic semiconductor is not doped: so, charges come from the electrodes and by changing the applied voltage we modify both the charge density and the charge profile within the organic film. Moreover, the organic semiconductors are strongly polarizable and the free charge carriers are polarons, or bipolarons, that can not be described as easily as the quasi-electrons or quasi-holes of Si [24,25]. Nevertheless, we verify that for sufficiently strong $V_{dc}$, charges have been accumulated at the pentacene/oxide interface and the junctions tend to the full accumulation regime where the capacitance is given by the one of the oxide only that is shown in Fig. 2. However, the full accumulation regime is not reached in the potential range that we have investigated: our data shows a transition region between depletion and accumulation much smoother than the one commonly observed in Si based MOS junctions that could be due to the differences between the free charges found in these two systems [11,12]. In decreasing $V_{dc}$ the carrier density decreases (Fig. 2) and drives continuously the system from the accumulation to the full depletion (starting from $V_{dc} = -5$ V). Finally for small enough potential values the organic layer is well free of charges and reacts as a dielectric. In this regime the equivalent capacitance corresponds to the series of oxide and pentacene capacitances which is lead to a pentacene dielectric constant of about 3.5, in agreement with values recently reported in literature [26]. It should be stressed that, as commonly observed for organic field effect transistors, our junctions are not ambipolar (p-semiconductor). Even after applying a strong negative potential ($V_{dc} < -40$ V) the capacitor remains in the depletion regime: no negative charges are accumulated at the interface.

### 3.2. Dipolar contributions

The two first contributions of the dielectric susceptibility (Eq. (2)) are of dipolar type. In general, the term dipolar should be understood in a broad sense referring to the frequency range where the responses take place. They are associated to particular entities that could be permanent dipoles carried by impurities present in the structure [17,18] or traps that can be successively charged and discharged [27], for instance. In our cases, we argue (as explain below) that the two dipolar contributions are likely to be caused by permanent dipoles, $\vec{\mu}_{SiO_2}$ and $\vec{\mu}_{Organic}$, located in the oxide and in the organic film, respectively. The origin of these dipoles remains to be clarified but they could be due, for instance, to substitution atoms coming from the doped silicon to the oxide and adsorbed polar molecules – such as water molecules – at the organic/oxide interface, respectively. In all cases, the permanent dipoles are driven out of their equilibrium position by the electric field and oscillate under the action of $V_{ac}$ giving contributions to the polarization. These motions can be modeled in terms of damped harmonic oscillators [17,18]. With this formalism, it was shown in Ref. [17] that the characteristic frequency of each oscillator depends on the dc electric field in the following way

$$1/\tau_{SiO_2/Organic}(\omega) \propto \vec{\mu}_{SiO_2/Organic}\vec{E}_{local}. \quad (3)$$

$\vec{E}_{local}$ is the electric field seen by the dipole considered. We have to include in Eq. (3) the local electric field instead of the applied field as done in Ref. [17], because the polarons

may screen the applied potential. According to this equation, the behaviors of the characteristic frequencies as function of $V_{dc}$ give information about the dipole orientation and the electrostatic properties of the junctions. Moreover, the permanent dipoles are not isolated systems but instead interact with their surroundings that could be materialized by the vibration modes of the junctions, for instance. These interactions cause energy dissipation and the characteristics of the surroundings (the bath) influence the dynamical properties of the oscillators [17,18]. Roughly speaking, if the bath has the faculty to forget instantaneously the perturbations induced by the oscillators (compared to the characteristic time of observation) [28], the dielectric susceptibility will be of Debye type. On the contrary, if the bath possesses a long term memory of these perturbations [28], the time response of the oscillators will be slow down that shows up in the dielectric susceptibility as fractional power laws. This is a Jonscher type of response [15] that could be modeled by several empirical functions [19,29,30]. In our junctions the two types of response are observed depending on the location of the oscillators.

A single dipolar contribution is seen in the admittance of the "reference" junctions. It is of Debye type

$$\chi_{SiO_2}(\omega) = A_{SiO_2}(1 - j\omega\tau_{SiO_2})^{-1}. \quad (4)$$

$A_{SiO_2}$ is the amplitude, proportional to the density of such dipoles [17]. $\tau_{SiO_2}$ is the characteristic relaxation time of these dipoles that is found between $10^{-5}$ and $10^{-7}$ s depending on cases. Two examples that differ by their characteristic relaxation time are shown: a first one in Fig. 1 with $\tau_{SiO_2} \approx 10^{-6}$ s, and a second one in Fig. 3 with $\tau_{SiO_2} \approx 10^{-5}$ s. As a remark we may notice that the loss part of the admittance, $C''$, of the two examples differ by one order of magnitude: in case of Fig. 1, as already stressed, it is close to the sensitivity limitation of our experiment what explains the wide fluctuations observed in the data. In all cases, the amplitude, $A_{SiO_2}$, and the characteristic frequency, $1/\tau_{SiO_2}$, do not vary with $V_{dc}$.

In the case of the organic MOS junctions, in the accumulation regime, the dielectric response of the organic thin film is strongly dominated by the one of the free carriers. As a consequence, again the bulk of the oxide only is probed and indeed, we obtain the same response (see Fig. 4a and b) where the two parameters of Eq. (4), $A_{SiO_2}$ and $\tau_{SiO_2}$, are potential independent with fixed values at all $V_{dc}$: $A_{SiO_2} \approx 7 \times 10^{-9}$ and $1/\tau_{SiO_2} \approx 2 \times 10^{6}$ Hz for the example shown in Figs. 1 and 4. Surprisingly, the characteristic frequency is the same for the reference and MOS junctions. As a remark, we may notice that the same kind of response was already obtained in the past for MOS capacitors that was interpreted in terms of charging and discharging of surface states [31]. First, since the reference junctions are of metal/oxide/metal type, the response should concern different kind of impurities located deep in the bulk and then not accessible by tunneling. Furthermore, the fact that the characteristic frequency is electric field independent is not consistent with such scenario, whereas independent permanent dipoles located in the bulk of the oxide would be a good assumption if we add an hypothesis concerning their orientation in space. The data correspond to the sum of the responses of all of them. According to Eq. (3), it then means that there is no preferential orientation for the permanent dipoles carried by these defects: they can take all accessible orientations in space with equal probability. Therefore, for some of them, the characteristic frequency will increase with the electric field, for some others, it will decrease, giving in total a field independent behavior.

As usual in MOS capacitor, the organic/oxide interface is probed when the junction is driven from accumulation to depletion regime. Decreasing progressively the voltage from accumulation, a second dipolar contribution appears at lower frequencies (see Fig. 1 from $10^2$ to $10^4$ Hz). It is of Jonscher type and well described by the Cole–Cole susceptibility

$$\chi_{Organic}(\omega) = A_{Organic}(1 + (-j\omega\tau_{Organic})^{\alpha})^{-1} \quad (5)$$

where $0 < \alpha < 1$ [19]. The amplitude, $A_{Organic}$, the characteristic frequency, $1/\tau_{Organic}$, and $\alpha$ ($\approx$0.5) change slightly with $V_{dc}$. We discuss in the following only the changes of characteristic frequencies from which we are able to obtain some information. An example is given in Fig. 5. First, we remark that our data can not be produced by successive

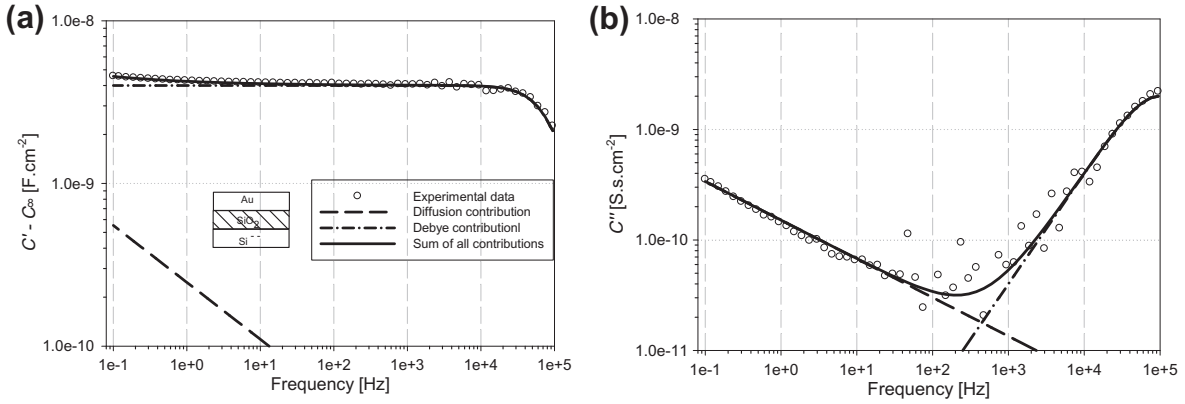


**Fig. 3.** Typical capacitance of a "Reference" $Si^+/SiO_2/Au$ (a) real part, (b) imaginary part at $V_{dc}$ = 0 V. The experimental data are fitted with two contributions: a Debye contribution for $SiO_2$ defects Eq. (3) and a LFD contribution for ion diffusion in the oxide Eq. (6). The fitting parameters are $A_{SiO_2} = 4 \times 10^9$; $\tau_{SiO_2} = 10^5 s$, $A_{Ion} = 5 \times 5\ 10^{-10}$ and $\beta = 1$.

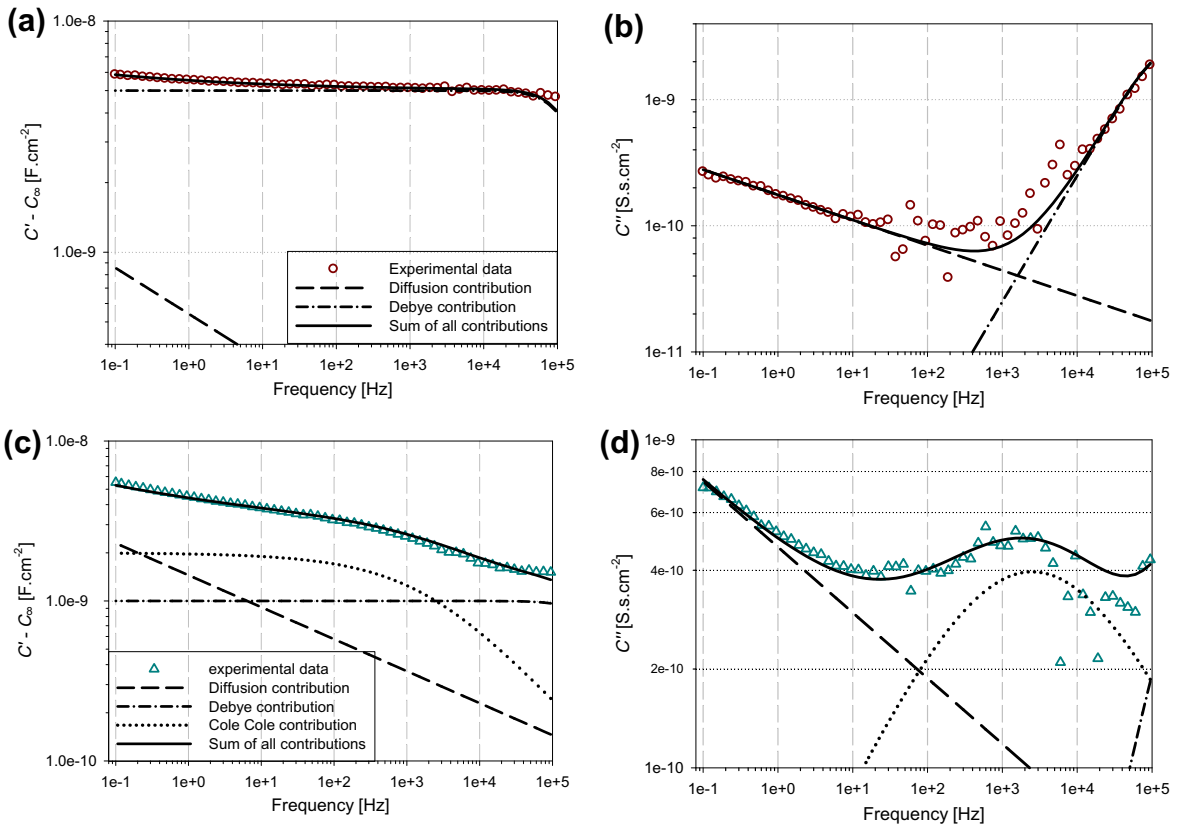


**Fig. 4.** Focus on two particular examples of Fig. 1 at $V_{dc} = +20$ V (a) real part, (b) imaginary part, and at $V_{dc} = -20$ V (c) real part, (d) imaginary part. The experimental data are fitted with two or three contributions: a Debye contribution for $SiO_2$ defects Eq. (3) – doted-dashed lines, a Cole–Cole contribution for organic defects Eq. (4) – doted lines, and a LFD contribution for ions at the $SiO_2$/pentacene interface Eq. (6) – doted line. The values of the parameters are discussed in the text.

charges and discharges in traps. Indeed, in this case the electric charges should come from the organic semiconductor and this contribution is also seen in the complete depletion regime where no free carriers are present in the pentacene film. In these conditions, the dipolar contribution can not be attributed to traps but, instead, is likely due to permanent dipoles. With this assumption and at the light of Eq. (3), the variations of $1/\tau_{Organic}$ seen in Fig. 5, indicate that the projection of the corresponding permanent dipoles is directed toward the substrate. Moreover, we clearly see different behaviors between the depletion regime ($V_{dc} < -5$ V), where the variations are linear, and the transition to the accumulation regime ($V_{dc} > -5$ V), where non-linearities are evidenced. These changes could be explained by the modification of the electrostatic properties of the junction induced by the formation of the space charges: the local electric field of Eq. (3) is progressively screened by the free carriers accumulated in the organic film. Notice that Fig. 5 is limited to the negative values of the dc potential for simplicity because this is the region where the Cole–Cole contribution is more pronounced.

### 3.3. Ionic contributions

The last contribution of the dielectric susceptibility (Eq. (2)) is a LFD type of contributions which is usually attributed to diffusion current of slow charges [21]. Moreover, in some heterostructures it was shown to be related to adsorbed water layer on one of the interfaces in the inside of the structure [21]. Under ambient condition such layer is expected to be formed in our systems at the surface oxide: water molecules is known to diffuse through the organic film [9]. They would then react with the Si–OH bonds present at the surface. This layer is supposed, on the one hand, to be at the origin of the Cole–Cole contribution Eq. (5) as discussed above and, on the other hand, to be the source of electrochemical reactions such as the one proposed in Refs. [9,10] that could be a possible origin to the LFD as explained in details below. When hole polarons (h) – or simply hole in the case of the reference junctions – are accumulated at this interface, protons are produced according to the coupled reactions $2H_2O + 4\,h \rightarrow 4H^+ + O_2(g)$ and $2H^+ \rightarrow 2\,h + H_2(g)$. The protons $H^+$ then migrate through the oxide, probably in the $H_3O^+$ state. The diffusion of particles through amorphous systems is known to follow, in general cases, a continuous time random walk in which the ions may remain after each jump at the same position for infinitely long time [32,23]. This type of random walk can be described by the fractional diffusion equation [23,33] characterized by a parameter $\beta$ ($0 \leqslant \beta \leqslant 1$), the case $\beta = 1$ corresponding to normal diffusion considered in Refs. [9,10]. This parameter controls

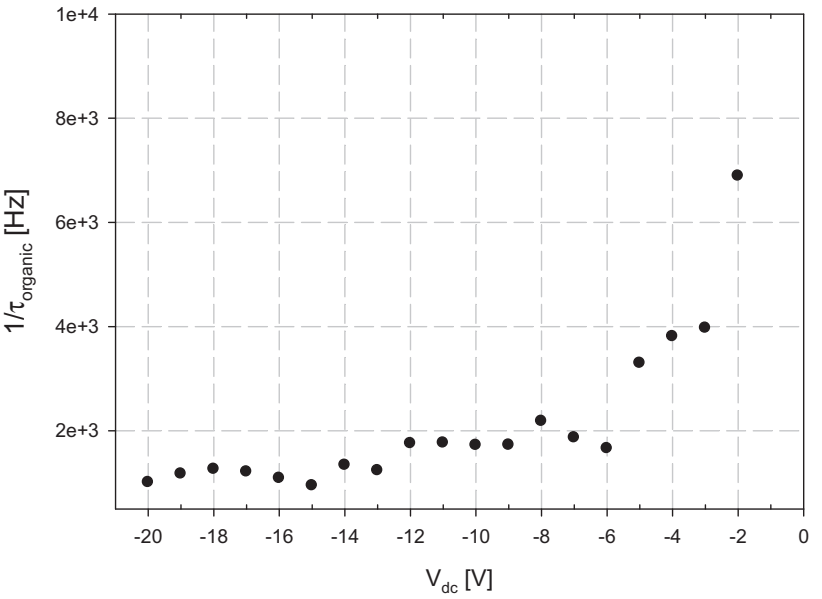


**Fig. 5.** $1/\tau_{organic}$ as function of $V_{dc}$: a change of behavior may be noticed between the depletion regime ($V_{dc} < -5$ V) and the transition to the accumulation regime ($V_{dc} > -5$ V).

the dynamics of the ions and can be measured in our experiment.

Because of the diffusive intrusion of protons in the oxide the capacitance becomes a function of time, C(t). The time needed for an ion to cross the oxide layer can be estimated to $10^7$ s, by taking $K_1 \approx 2 \times 10^{-19}$ cm$^2$ s$^{-1}$ given in Ref. [10], but is certainly longer for anomalous diffusion. As a consequence, during the time of our experiment, the protons remain very close to the interface and we may reasonably assume that the changes of capacitance are a linear function of the amount of ions inside the oxide. Taking the time derivative, we may then write (see Appendix A)

$$\dot{C}(t) = -A_C J_\beta(0,t) \tag{6}$$

$J_\beta$ is the anomalous diffusion current of protons taken at the interface ($x = 0$) and the constant $A_C$ takes account for the effects of the ions on the capacitance. According to Eq. (6), the dielectric susceptibility of the LFD is directly related to the admittance of the ionic anomalous diffusion, $Y_{Ion}$, which was calculated in Refs. [22,34]. In the limit of high frequencies (compared to the characteristic frequency $10^{-7}$ Hz for ion diffusion) that corresponds to our experiments, we finally obtain:

$$\chi_{Ion}(\omega) = -\frac{A_c}{j\omega} Y_{Ion}(\omega) \approx A_{Ion}(-j\omega)^{-\beta/2} \tag{7}$$

that reproduces very well our data (Figs. 3 and 4). The detailed expression of the amplitude $A_{Ion}$ can be found in the Appendix A. For the reference junctions we get $\beta = 1$ that corresponds to normal diffusion (see Fig. 3). For the organic based junctions we find anomalous diffusion with $\beta$ between 0.2 and 0.4. In the example of Fig. 4, the Cole–Cole contribution is strong enough to spoil the characteristics

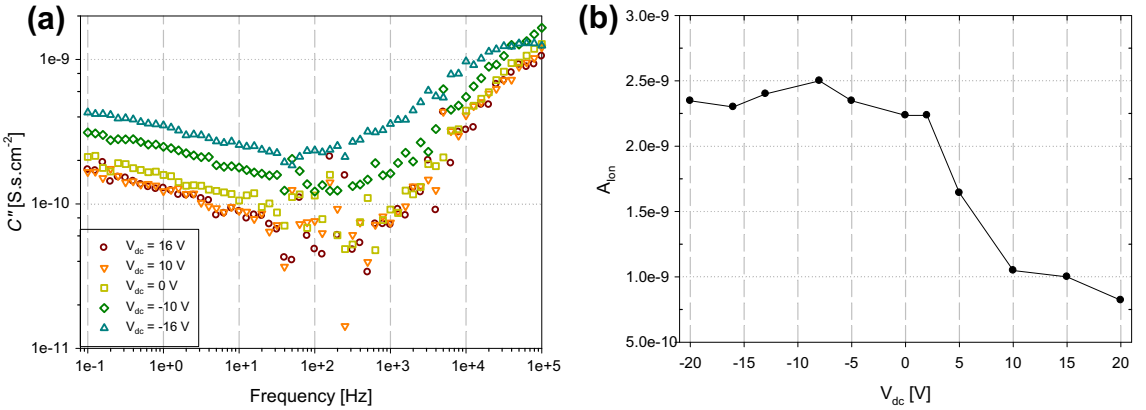


**Fig. 6.** (a) $C''$ for a junction with a weak Cole–Cole contribution showing more clearly the LFD contribution at all $V_{dc}$: some examples are shown from the accumulation to the depletion regime. The $\beta$ parameter is bias independent – in this case $\beta = 0.3$, and the amplitude of the ionic contribution increases when $V_{dc}$ decreases. (b) Amplitude of the ionic contribution, $A_{Ion}$, as function of $V_{dc}$ for the example shown in Figs. 1 and 4.

of the LFD contribution that are more apparent in some other examples such as the one shown in Fig. 6a. We find $\beta = 0.4$ in the example of Fig. 4 and $\beta = 0.3$ in the example of Fig. 6a. Moreover, we notice that the amplitude, $A_{Ion}$, increases when $V_{dc}$ decreases in a way shown in Fig. 6b that corresponds to the junction investigated in Figs. 1 and 4. According to Eq. (A12) of the Appendix A, $A_{Ion}$ is inversely proportional to the proton density at the interface. With the chemical reactions described above that explain the mechanism of proton production, this density is directly related to the density of holes accumulated at the interface – a linear relation between these two quantities is assumed in Ref. [10]. Following this assumption, $A_{Ion}$ becomes inversely proportional to the density of holes at the interface. This is in agreements with our findings (Fig. 6b): in the depletion regime, the hole density is very weak and $A_{Ion}$ is maximal, on the opposite, in the accumulation regime, the hole density increases implying a decrease of $A_{Ion}$. The reasons why the diffusion characteristics are different in the two types of junctions remain unclear. It may be explained by the structural characteristic of the two interfaces, Au/oxide and pentacene/oxide, that should be very different. However, we do not have clear ideas on the way a particular structural organization influences the proton diffusion.

## 4. Conclusions

In summary, we have measured the low frequency admittance of metal/oxide/organic semiconductor junctions and identified both dipolar and diffusive current contributions to the polarization. The dynamical responses of the polarizable species (dipoles or ions) are strongly influenced by their surroundings. If they are markovian (without memory) we get a Debye response for the dipoles and a normal diffusion for the ions as measured for "reference" junctions. If they are non-markovian (with memory) the responses are more complex; in their simplest forms we get a Cole–Cole response for the dipoles and a fractional diffusion for the ions. Our data show anomalous behavior in presence of organic layer. We believe these observations could be the signature of particular structural organizations which can be located either, in the organic layer itself or, in the organic/oxide interface.

## Acknowledgements

We thank Nicolas Clement for fruitful discussion and the Region Champagne-Ardenne for financially supporting of PhD of Romuald Ledru. This work has been supported by the ANR under contract No. ANR-09-BLAN-0329-02 (CADISCOM).

## Appendix A. Model for the anomalous Low Frequency Dispersion (LFD)

We note $p(x, t)$ the time dependant volume density of protons in the oxide at distance $x$ from the organic/oxide interface. The thickness of the oxide layer is $L \approx 70$ nm. As it is usual for amorphous systems, the protons are assumed to follow a continuous time random walk through the oxide [31,23]. It means that after each jump the protons may remain at the same position for infinitely long time. In practice this could happen in deep traps. This type of random walk can be described by the fractional diffusion equation [33]

$$\frac{\partial p(x,t)}{\partial t} = {}_0D_t^{1-\beta} K_\beta \frac{\partial^2 p(x,t)}{\partial x^2} = \frac{K_\beta}{\Gamma(\beta)} \frac{\partial}{\partial t} \int_0^t dt' \frac{1}{(t-t')^{1-\beta}} \frac{\partial^2 p(x,t')}{\partial x^2}. \quad \text{(A1)}$$

${}_0D_t^{1-\beta}$ is the fractional Riemann–Liouville operator with definition given by the second equality of Eq. (A1), $\beta$ is a constant such that $0 \leqslant \beta \leqslant 1$, $\Gamma$ is the Gamma function and $K_\beta$ generalizes the diffusion coefficient with dimension $cm^2 \cdot s^{-\beta}$. The case $\beta = 1$ corresponds to normal diffusion. This density should also fulfill the charge conservation equation

$$\frac{\partial p(x,t)}{\partial t} = \frac{\partial J_\beta(x,t)}{\partial x}. \quad \text{(A2)}$$

$J_\beta$ is the anomalous diffusion current of protons that may be written as [35]

$$J_\beta(x,t) = -q \frac{K_\beta}{\Gamma(\beta)} \times \frac{\partial}{\partial x} \left[ t^{\beta-1} p(x,0) + \int_0^t dt' p(x,t')(t-t')^{\beta-1} \right]. \quad \text{(A3)}$$

$q$ is the electric charge of the diffusing ions. On the contrary to normal diffusion ($\beta = 1$), the current is non-local in time: at each time it depends on the previous history. Moreover, the first term of Eq. (A3) shows that the initial condition contributes at all times.

Because the protons diffuse through the oxide, the capacitance of our junction becomes time dependant, $C(t)$. The proton diffusion is very slow: it takes about $10^7$ s for an ion to cross the oxide so that during the time of our experiments, they all remain close to the organic/oxide interface [10]. We therefore suppose

$$C(t) = C(0) - A_C \int_0^L dx p(x,t). \quad \text{(A4)}$$

The ions modify the capacitance by Coulomb interaction but since the ions are all approximately at the same distance from the interface the complicated space dependence due to these interactions may be reduced to a single constant $A_C$. Taking the time derivative of Eq. (A4) and with the help of the charge conservation equation (Eq. (A2)) we obtain

$$\dot{C}(t) = -A_C J_\beta(0,t). \quad \text{(A5)}$$

The dot is for the time derivative. We have considered that $J_\beta(L,t) = 0$ since all the ions remain near $x = 0$.

The ions continuously diffuse through the oxide. Applying in addition a small ac potential introduces a perturbation to the main contribution. We write

$$p(x,t) = p_0(x,t) + p_1(x,t). \quad \text{(A6)}$$

$p_0$ is the dc component, $p_1$ the ac perturbation. In the same way we can decompose the surface potential at the organic/oxide interface

$$\psi(t) = \psi_0(t) + \psi_1(t). \tag{A7}$$

To determine the admittance associated to the ion displacement we need to consider only the ac components; $p_0(x,t)$ and $\Psi_0(t)$ may indeed be considered as time independent in the time spend to do the experiments. Taking the Laplace transform of Eq. (A5) yields

$$\chi_{Ion}(s) = -\frac{A_C}{s} Y_{Ion}(s) \tag{A8}$$

where the admittance of the ionic current is defined as

$$Y_{Ion}(s) = \frac{\tilde{J}_\beta(0,s)}{\tilde{\psi}_1(s)}. \tag{A9}$$

$\tilde{J}_\beta(0,s)$ and $\tilde{\psi}_1$ are the Laplace transforms of the diffusion current, $J_\beta$, at $x = 0$ and of $\Psi_1$, respectively. Eq. (A9) was solved in Ref. [22] assuming a linear relation between $p_1(x,t)$ at the interface and $\Psi_1(t)$. With ideal conditions for the electrochemical reaction it may be written [34]

$$\Psi_1(t) = \frac{k_B T}{p_0(0,0)} p_1(0,t). \tag{A10}$$

$T$ is the temperature and $k_B$ the Boltzmann constant. Different boundary conditions at the other interface were considered by the authors of Ref. [22] but, it is important to stress that at the frequencies we consider in this work they do not play any role. We quote their solution for absorbing boundary conditions, $p_1(L,t) = 0$. In terms of frequency instead of Laplace coordinate we finally get

$$\chi_{Ion}(\omega) = -\frac{A_c}{j\omega} Y_{Ion}(\omega) = \frac{q k_B T K_\beta}{L} \frac{\omega_d^{1-\beta}}{p_0(0,0)} \left[\frac{-j\omega}{\omega_d}\right]^{-\beta/2} \times \frac{1}{\tanh((-j\omega/\omega_d)^{\beta/2})} \tag{A11}$$

With $\omega_d = (K_\beta/L^2)^{1/\beta}$. At high frequencies, $\omega/\omega_d \to +\infty$, this equation gives

$$\chi_{Ion}(\omega) \approx q \frac{k_B T K_\beta}{L} \frac{\omega_d^{1-\beta}}{p_0(0,0)} \left[\frac{-j\omega}{\omega_d}\right]^{-\beta/2} = A_{Ion}(-j\omega)^{-\beta/2} \tag{A12}$$

that corresponds to Eq. (7) of the main text. It would be the same with open boundary conditions, for instance.

## References


[1] H. Sirringhaus, Adv. Mater. 21 (2009) 3859.
[2] A.R. Brown, C.P. Jarrett, D.M. de Leeuw, M. Matters, Synth. Met. 88 (1997) 37.
[3] J.B. Chang, V. Subramanian, Appl. Phys. Lett. 88 (2006) 233513.
[4] A. Salleo, F. Endicott, R.A. Street, Appl. Phys. Lett. 86 (2005) 263505.
[5] M. Tello, M. Chiesa, C.M. Duffy, H. Sirringhaus, Adv. Funct. Mater. 18 (2008) 3907.
[6] R.A. Street, M.L. Chaninyc, F. Endicott, B. Ong, J. Appl. Phys. 100 (2006) 114518.
[7] R.A. Street, A. Salleo, M.L. Chaninye, Phys. Rev. B 68 (2003) 085316.
[8] S.J. Zilker, C. Detcheverry, E. Cantatore, D.M. de Leeuw, Appl. Phys. Lett. 79 (2001) 1124.
[9] A. Sharma, S.G.J. Mathijssen, M. Kemerink, D.M. de Leeuw, P.A. Bobbert, Appl. Phys. Lett. 95 (2009) 253305.
[10] A. Sharma, S.G.J. Mathijssen, E.C.P. Smits, M. Kemerink, D.M. de Leeuw, P.A. Bobbert, Phys. Rev. B 82 (2010) 075322.
[11] E.H. Nicollian, A. Goetzberger, Bell Syst. Tech. J. 46 (1967) 1055.
[12] E.H. Nicollian, J.R. Brews, MOS (Metal Oxide Semiconductor) Physics and Technology, Wiley, New York, 1982.
[13] (a) N. Alves, D.M. Taylor, Appl. Phys. Lett. 92 (2008) 103312; (b) I. Torres, D.M. Taylor, J. Appl. Phys. 98 (2005) 073710.
[14] S. Grecu, M. Roggenbuck, A. Opitz, W. Brütting, Org. Electron. 7 (2006) 276.
[15] A.K. Jonscher, Nature (London) 267 (1977) 673.
[16] N. Clément, S. Pleutin, D. Guérin, D. Vuillaume, Phys. Rev. B 82 (2010) 035404.
[17] S. Pleutin, N. Clément, D. Guérin, D. Vuillaume, Phys. Rev. B 82 (2010) 125436.
[18] I. Goychuk, Phys. Rev. E 76 (2007) 040102R.
[19] K.S. Cole, R.H. Cole, J. Chem. Phys. 9 (1941) 341.
[20] G.G. Raju, Dielectrics in Electric Field, Marcel Dekker, Basel, New York, 2003.
[21] L.A. Dissado, R.M. Hill, J. Chem. Soc. Faraday Trans. 2 80 (1984) 291.
[22] J. Bisquert, A. Compte, J. Electroanal. Chem. 499 (2001) 112.
[23] (a) R. Metzler, J. Klafter, Phys. Rep. 339 (2000) 1; (b) J. Klafter, I.M. Sokolov, Phys. World 18 (2005) 29.
[24] N. Tessler, Y. Preezant, N. Rappaport, Y. Roichman, Adv. Mater. 21 (2009) 2741.
[25] S. Coropceanu, J. Cornil, D.A. da Silva Filho, Y. Olivier, R. Silbey, J.L. Bredas, Chem. Rev. 107 (2007) 926.
[26] C.H. Kim, O. Yaghmazadeh, D. Tondelier, Y.B. Jeong, Y. Bonnassieux, G. Horowitz, J. Appl. Phys. 109 (2011) 083710.
[27] (a) P.P. Boix, G. Garcia-Belmonte, U. Munecas, M. Neophytou, C. Waldauf, R. Pacios, Appl. Phys. Lett. 95 (2009) 233302; (b) T. Walter, R. Herberholz, C. Müller, H.W. Schock, J. Appl. Phys. 80 (1996) 4411.
[28] U. Weiss, Quantum Dissipative System, third ed., World Scientific, Singapore, 2008.
[29] D.W. Davidson, R.H. Cole, J. Chem. Phys. 19 (1951) 1484.
[30] S. Havriliak, S. Negami, Polymer 8 (1967) 161.
[31] M.J. Uren, S. Collins, M.J. Kirton, Appl. Phys. Lett. 54 (1989) 1448.
[32] H. Scher, E.W. Montroll, Phys. Rev. B 12 (1975) 2455.
[33] A. Compte, Phys. Rev. E 53 (1996) 4191.
[34] J. Bisquert, G. Garcia-Belmonte, F. Fabregat-Santiago, P.R. Bueno, J. Electroanal. Chem. 475 (1999) 152.
[35] D.H. Zanette, Physica. A 252 (1998) 159.